



Geophysical Research Letters

RESEARCH LETTER

10.1029/2019GL086721

Key Points:

- Extreme daily precipitation is strongly correlated with and on average amplified to twice the vertically integrated water vapor
- As water vapor increases there is evidence for nonlinear scaling at lower (higher) values of q with decreasing (increasing) amplification
- Vertical velocity and related weather types modulate the amplification along with complex terrain and along ocean/land transitions

Supporting Information:

- Supporting Information S1

Correspondence to:

K. E. Kunkel,
kekunkel@ncsu.edu

Citation:

Kunkel, K. E., Stevens, S. E., Stevens, L. E., & Karl, T. R. (2020). Observed climatological relationships of extreme daily precipitation events with precipitable water and vertical velocity in the contiguous United States. *Geophysical Research Letters*, 47, e2019GL086721. <https://doi.org/10.1029/2019GL086721>

Received 18 DEC 2019

Accepted 29 APR 2020

Accepted article online 10 MAY 2020

Observed Climatological Relationships of Extreme Daily Precipitation Events With Precipitable Water and Vertical Velocity in the Contiguous United States

Kenneth E. Kunkel¹ , Scott E. Stevens¹ , Laura E. Stevens¹ , and Thomas R. Karl²

¹North Carolina Institute for Climate Studies, North Carolina State University, Asheville, NC, USA, ²Climate and Weather, L.L.C, Mills River, NC, USA

Abstract An analysis of 3,104 stations in the United States shows virtually every station exhibits a positive correlation between precipitable water (PW) and extreme daily precipitation (EP) with over one-third statistically significant. To first approximation, EP scales linearly with PW, but there is nonlinear scaling at the lower and upper ends of the PW distribution. On average, EP is amplified by twice the amount of PW, but there is substantial seasonal and spatial variability caused by dynamically forced vertical velocity with stations ranging from a one-to-one relationship to over three-to-one. These latter stations are generally found in elevated terrain or near coasts and in regions and seasons affected by strong synoptic-scale weather systems. The results also point to PW, not vertical velocity, as the key limiting factor in the most intense EP events. This has important implications for projecting changes of the most intense EP events in a warmer world.

Plain Language Summary As the climate warms, water vapor is increasing in the atmosphere. Analysis of the historical observations of extreme daily precipitation shows that precipitation amounts increase with more water vapor in the atmosphere. On average, extreme daily precipitation amounts equate to twice the amount of water vapor. There is, however, considerable spatial and seasonal variability affected by the predominant weather types in the region, orography, and proximity to oceans. The analysis indicates that when the amount of atmospheric water vapor is high, as occurs during the warm season and in the south and eastern portions of the United States, the increase in extreme precipitation for a given increase in water vapor becomes disproportionately large compared to the same increase at low amounts of water vapor. Water vapor is a limiting factor in the amount of extreme precipitation more often than the intensity of the weather causing the event.

1. Background and Motivation

Numerous analyses and scientific assessments have documented observed increases in both extreme precipitation frequency and magnitude across the United States and in many other regions (Easterling et al., 2017; Groisman et al., 2005; Hoerling et al., 2016; IPCC, 2013; Karl & Knight, 1998; Kunkel et al., 2020). Nonetheless, the rates of extreme precipitation change have considerable spatial variability, and not all areas show increases. Understanding the causes of these differences is critically important for infrastructure investment that rely on extreme precipitation design criteria (Kunkel et al., 2013; Wright et al., 2019). Many users in the United States rely on NOAA's Atlas 14 and various updates from Volumes 1 to 11 (Bonnin et al., 2004; Perica et al., 2018) to accurately reflect the probability of extremes during infrastructure lifetimes. Compounding the challenge of estimating future extreme precipitation design values are the ongoing and projected changes in climate (IPCC, 2013) as the world warms.

There is a strong thermodynamic relationship between temperature and water vapor (q) given by the Clausius-Clapeyron (CC) equation. Climate models indicate that a disproportionate increase in extreme precipitation will occur compared to the change in the annual mean total precipitation (Sillmann et al., 2013). Since Trenberth et al. (2003) first proposed that in a warmer world additional latent heat release from the condensation of q could provide a positive feedback leading to super CC scaling, several studies have revealed important complexities related to scaling of the changes of the mean global and large-area temperature increases to increases in q and subsequent extreme precipitation amounts (Ban et al., 2015; Bao,

©2020 The Authors.

This is an open access article under the terms of the Creative Commons Attribution-NonCommercial License, which permits use, distribution and reproduction in any medium, provided the original work is properly cited and is not used for commercial purposes.

Sherwood, Colin et al., 2017; Boessenkool et al., 2017; Chan et al., 2016; Huang et al., 2019; Schroeer & Kirchengast, 2018; Wang et al., 2017). Additionally, changes in weather dynamics associated with new climatological weather regimes further complicate projections of extreme precipitation changes as the world warms through altered fields of vertical velocity (VV) and moisture convergence (Nie et al., 2018; O'Gorman & Schneider, 2009; Prein & Pendergrass, 2019; Sugiyama & Shiogama, 2010). This can manifest itself in various ways including: the size and location of areas that become moisture limited, the frequency and intensity of strong short-duration versus weaker long-duration convective events, and changes in local temperatures during extreme event downdrafts and updrafts (Bao, Sherwood, Alexander, et al., 2017; Giorgi et al., 2019; Kitoh & Endo, 2016; Kunkel et al., 2012; Nie et al., 2018; O'Gorman & Schneider, 2009; Thackeray et al., 2018).

Given these complexities, a direct climatological analysis between extreme precipitation and q , bypassing the complexities of local to global temperature changes, could help our understanding of the climatological roles of q and dynamics. Specifically, the thermodynamic effects are addressed by analyzing vertically integrated q (precipitable water, PW), foregoing temperature to PW estimates. Some studies have explored PW climatology with extreme precipitation events outside of the United States (e.g., Dong et al., 2019; Huang et al., 2019; Lavers et al., 2016; Ye et al., 2015, 2017a, 2017b), but there has been a dearth of analyses covering the contiguous United States. This is particularly relevant as PW is increasing in the United States and is projected to increase globally (Kunkel et al., 2013, 2020). Additionally, dynamic effects are explored through VV and associated weather.

2. Data and Methods

The United States has spatially dense high-quality daily data sets of precipitation. PW and VV are available through model reanalysis fields. Additionally, this region provides a rich diversity of complex terrain and seasonally and spatially varying weather types, which play an important role in extreme precipitation intensity (Emori & Brown, 2005; Kunkel et al., 2012; Mahoney et al., 2018).

Data from the Global Historical Climatology Network-Daily (GHCND; Menne et al., 2012) were used to identify 3,104 stations with less than 10% missing precipitation data over the period 1949–2017. This data set has undergone extensive quality control (Durre et al., 2010; Durre et al., 2008), and the large spatial and temporal sample size is a major advantage compared to more limited hourly data sets. Many of the GHCND stations are part of the U.S. Cooperative Observer Network (“COOP”) with its characteristic once-a-day manual observation that has varied by observer and changed over time (Karl et al., 1986). A systematic shift in COOP station observation times (e.g., once a day observations changing from afternoon to morning) could introduce an offset between the extreme daily precipitation (EP) event and the PW and ω data, leading to additional measurement uncertainty. However, an analysis of EP and PW using virtually the same set of stations found no apparent systematic time-dependent biases (Kunkel et al., 2020).

Two similar EP metrics were computed for each station. First, the time series of the yearly maximum daily precipitation, or annual maximum series (AMS), is the starting point for many analyses of intensity-duration-frequency (IDF) relationships (Bonnin et al., 2004). Second, the amount of precipitation on those days exceeding the 1-yr, 1-day recurrence threshold, the partial duration series (PDS), consists of the highest 69 daily events for a station with a complete 69-year period of record. There was considerable overlap between these two metrics; on average, more than two thirds of the PDS and AMS values are the same events. The average PDS precipitation amount is greater than the AMS, but the largest event in the series represents a return interval of more than 50 years.

Maximum daily 3-hr values of PW and VV in pressure coordinates (ω) were derived from the National Centers for Environmental Prediction (NCEP)/National Centers for Atmospheric Research (NCAR) reanalysis (Kalnay et al., 1996) and NASA's MERRA-2 reanalysis (Gelaro et al., 2017). MERRA-2 data only extend back to 1980, compared to 1949 for the NCEP/NCAR reanalysis. Other differences include: data assimilation methods, models, data sources, time resolution (NCEP/NCAR 3-hourly and MERRA-2 hourly), and spatial resolutions (NCEP/NCAR: $2.5^\circ \times 2.5^\circ$, and MERRA-2: $0.5^\circ \times 0.625^\circ$). The longer NCEP/NCAR reanalysis was used as the primary reanalysis data set, while MERRA-2 was used to help assess the robustness of relying on the NCEP/NCAR reanalysis. Hereafter, the analysis and discussion will use the negative of ω ; thus, positive values indicate upward VV.

Some results are averaged across nine climate regions within the contiguous United States. The regions are coherent large-scale anomalies of moisture excess and deficit (Karl & Koscielny, 1982) bounded by geopolitical borders (supporting information Figure S1).

The concepts and terminology introduced and used by Emori and Brown (2005), O'Gorman and Schneider (2009), and Nie et al. (2018) provide a useful framework for evaluating EP scaling given by

$$EP \cong PW \Omega \Gamma \quad (1)$$

where Ω is a metric of the vertical velocity set to $-\omega$ at 500 hPa and Γ represents the vertical covariances of the standardized PW and ω , that is, the covarying vertical changes of ω and PW. However, as pointed out by O'Gorman and Schneider (2009) and supported by Nie et al. (2018), when the thermal structure of the atmosphere is moist adiabatic on synoptic scales, then Γ 's influence on EP variations is small and can be neglected. So in this analysis Γ is assumed to be 1. PW represents the thermodynamic contribution, while the dynamic component, ω , is strongly affected by specific weather types leading to upward VV. PW is the result of circulation from all weather types, independent of VV.

Thermodynamic effects are examined more closely through the amplification factor, \mathbf{A} , defined within specific PW intervals as

$$\mathbf{A}_s = \sum_{i=1}^N EP_{s,i} / \sum_{i=1}^N PW_{s,i} \quad (2)$$

where \mathbf{A}_s is the average amplification factor for station s , $EP_{s,i}$ is the precipitation magnitude for event i at station s , $PW_{s,i}$ is the precipitable water for event i at station s , and N is the number of extreme events at station s (69 annually and less seasonally). Annual and seasonal (warm and cold) averages of \mathbf{A} were calculated for each station and averaged for climate regions (Figure S1) and the contiguous United States. \mathbf{A} is affected by the combined effects of ω , any smaller effect of Γ , and the local terrain and wind fields not captured from the reanalyses.

3. Results

3.1. Regional Climatology of PW, ω , and EP

The PW probability distribution is shifted toward higher values on EP event days compared to all days, with higher values in the eastern and southern regions for both EP event days and all days (Figure 1). In addition, the moisture-limited regions of the western United States (West, Southwest, West North Central, and Northwest Regions) have less separation between the two PW probability distributions, in contrast to the other eastern regions.

In contrast to PW, the separation of the $-\omega$ distributions is greater in the far west (Northwest and West) with the peak frequency of $-\omega$ on EP days reaching 0.3 to 0.4 Pa s⁻¹ compared to other areas that peak around 0.2 Pa s⁻¹ (Figure S2). EP events in these regions are more likely to be observed with higher values of $-\omega$ compared to other regions (Figure S2).

Seasonally, higher PW is observed in all areas during the warm (May–October) season compared to the cold (November–April) season (Figure S3). All areas have higher $-\omega$ in the cold season compared to the warm season, including regions that are frequented by tropical cyclones, for example, the South, Southeast, and Northeast Regions (Figure S4). There are a few events in each region where $-\omega$ is 0 or slightly negative, suggesting some timing and/or accuracy errors in ω .

The median area affected by EP events increases exponentially with PW, growing from relatively small areas of roughly 10,000 km² for PW < 20 mm to over 75,000 km² for PW > 70 mm (Figure S5). This suggests that high local PW is usually associated with ample q over relatively large areas (Figure S5) for weather system triggering.

3.2. Linear and Nonlinear Thermodynamic and Dynamic Effects

A composite of all U.S. stations shows approximately that the mean and various quantiles of the 1-yr, 1-day EP event magnitudes increase monotonically with PW (Figure 2a) as might be expected from equation 1. This is clearly not the case for those events when stratified by $-\omega$ (Figure 2b). The highest values of EP

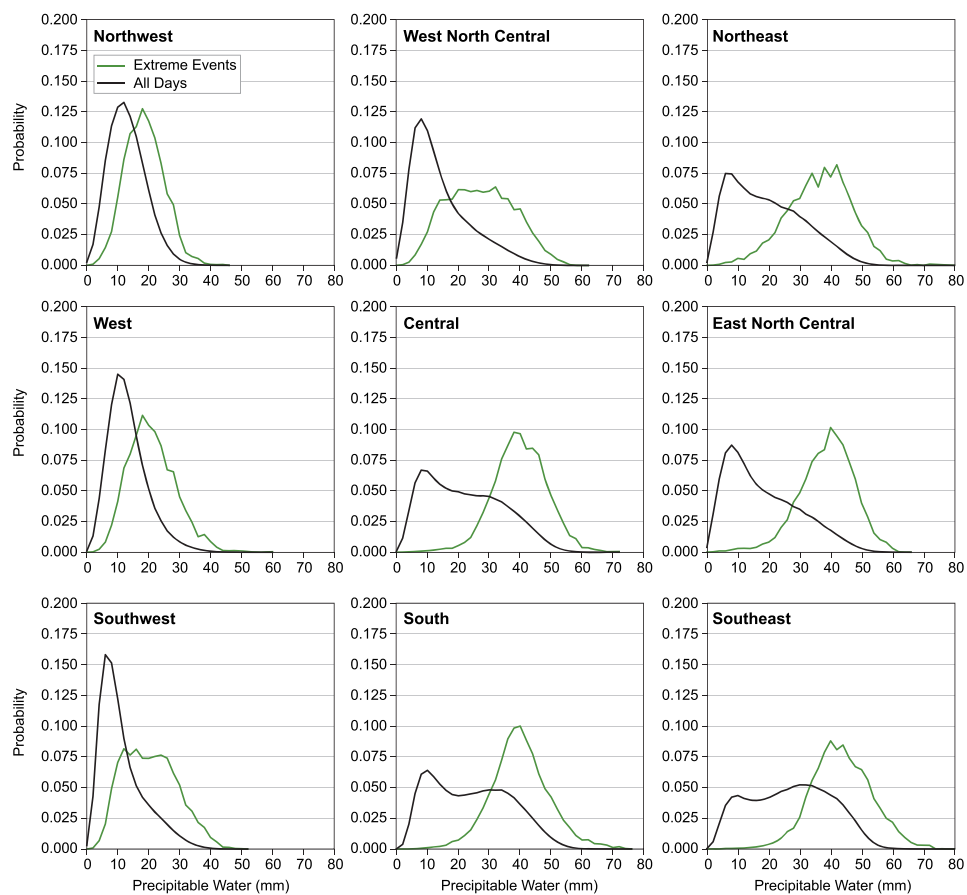


Figure 1. Annual fractional probability distribution of all days (black line) and days with an extreme (1-yr, 1-day recurrence) precipitation event (green line) versus precipitable water (the 3-hr maximum during the event day) in 2 mm increments by climate region.

are associated with the highest values of PW, but not the highest values of $-\omega$. This implies that (1) ω is not a limiting factor in EP magnitudes beyond a threshold value of PW, in contrast to PW, (2) PW and $-\omega$ are inversely related at high values of $-\omega$, or (3) a combination of both. The first point is addressed in this section, and the second point is evaluated in section 3.3.

The PW-EP relationship is illuminated by an examination of **A**. **A** averages about 2 and could be interpreted as the equivalent of the atmosphere turning over twice during an EP event day. However, it is dependent on PW (Figure 2c), with higher (lower) values at lower (higher) PW. A set of Monte Carlo simulations (see supporting information—Monte Carlo) was tested for EP versus PW nonlinearity for both the PDS (Figure 2c) and AMS (Figure S6). Results confirm that nonlinear scaling occurs at both the lower and higher portions of the PW distribution for both reanalyses (Figure S7). Additionally, for very high EP amounts, the amount of PW is limiting, not $-\omega$. Sample size of the highest PW bin (321) is below the minimum (700) recommended by Boessenkool et al. (2017), suggesting that the highest bin pair comparison is less robust, although it is consistent with the adjacent bin pair.

The high **A** values for low PW are not necessarily true considering all precipitation events. In the subset of precipitation events used here, very strong dynamics, and consequently high or unusually sustained $-\omega$, is necessary at low PW (e.g., 20 mm) to achieve the EP event threshold. The decrease in **A** as PW increases is attributed to less stringent limits on VV to achieve the thresholds. In contrast, the statistically significant increases of **A** at high PW are not likely due to higher $-\omega$ because the highest PW values occur during the warm season when $-\omega$, spatially averaged over reanalysis grid boxes, tends to be lower. Although less likely, because of the PW averaging across regions and seasons, the dynamics might also be adding to the effect, for example, warm season tropical storms. But Figure S8 shows that nonlinear scaling at high PW

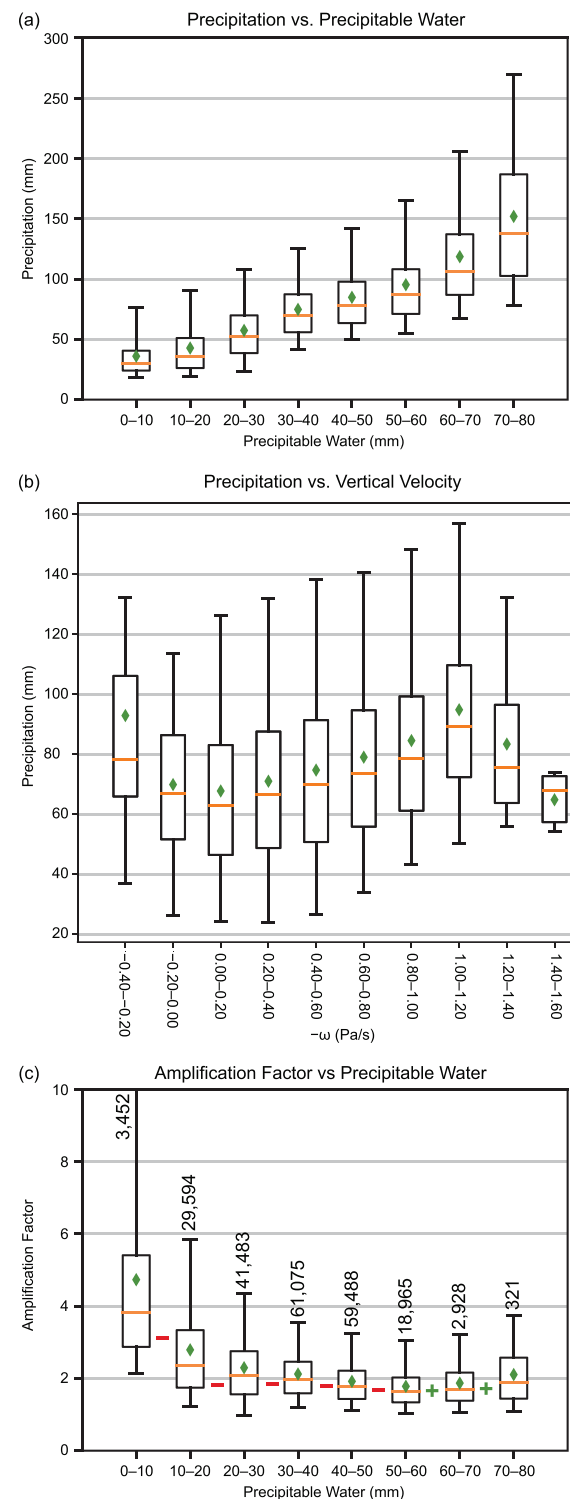


Figure 2. Boxplot distributions for the 1-yr, 1-day PDS of (a) precipitation event amount versus the same-day 3-hr maximum PW sorted into 10 mm interval bins; (b) as in panel (a) but for $-\omega$, and (c) as in panel (a) but for the amplification factor \mathbf{A} (EP/PW). Boxplots display mean (green diamonds), median (orange horizontal lines), 25th and 75th percentiles (box limits), and 5th and 95th percentiles (whiskers). “-” and “+” denote a significant decrease and increase (0.05 level), respectively, of the difference (higher bin minus lower bin) of \mathbf{A} between adjacent PW intervals. The observation count used in the statistical tests is depicted above the top whisker, and the 95th percentile value for bin 0–10 is 10.75 (panel c).

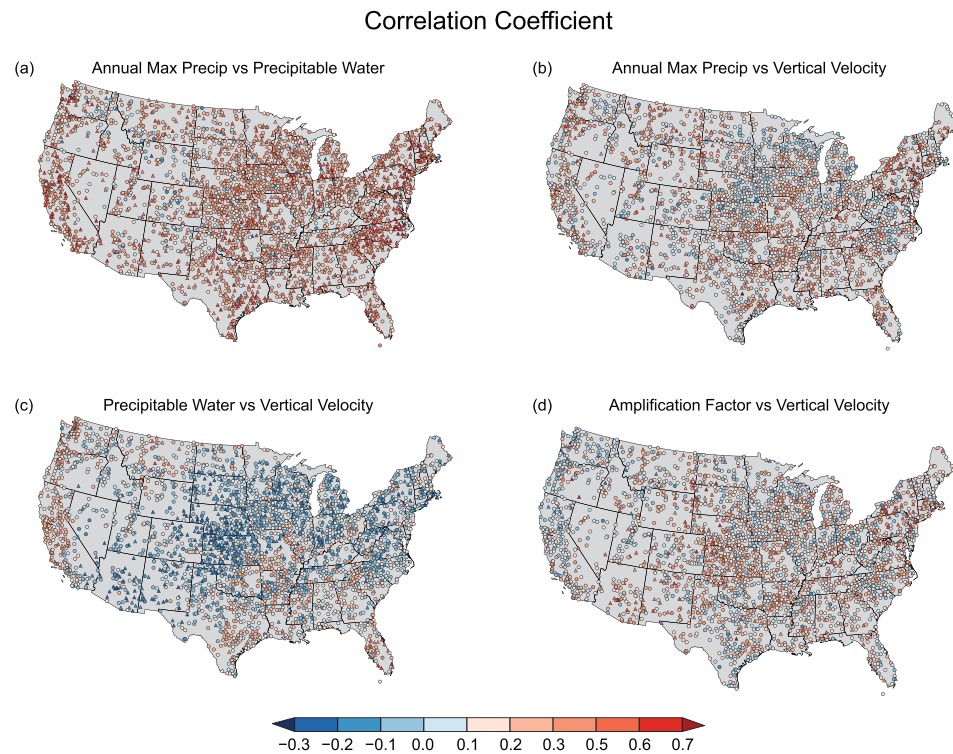


Figure 3. Correlation coefficients for the AMS of (a) EP event magnitude with PW, (b) EP event magnitude with $-\omega$, (c) PW with $-\omega$, and (d) \mathbf{A} with $-\omega$. PW and $-\omega$ are the simultaneous day's 3-hr maximum precipitable water and 3-hr maximum vertical velocity, respectively. Triangles indicate statistically significant (0.05 level) correlations (two-tailed t test).

is mostly attributed to the Northeast and Southeast where PW and associated EP are highest (Figure 1). This effect is also evident in the South and Central Regions at the highest PW values. Nonetheless, from these diagnostics it is not possible to completely rule out high values of ω during tropical cyclones, for example, as partially contributing to the apparent nonlinear relationship. The spatial relationships among the various variables is explored in section 3.3 to help discriminate among the roles of PW and ω with EP events.

3.3. Spatial Variability of EP, PW, and ω

The relationships of EP event magnitude versus local PW and ω are potentially complex (Figures 2b and 2c). Simple correlation coefficients are used to better understand this complexity. For most stations, the 69 EP events increase in magnitude as PW increases (Figure 3a), independent of which reanalysis is used (Figure S9). Stations with negative correlations are primarily located in western intermontane areas. The coastal areas of the West Region as well as the Cascade and Sierra Nevada Mountains tend to have the highest positive correlations with lower, even negative, correlations immediately to the east (favored downslope areas). Central and eastern regions are dominated by positive correlations with over one third of the stations statistically significant (Table S1). By contrast, there are large areas with negative correlations between EP and $-\omega$ and relatively few (less than 10%) statistically significant positive correlations (Figure 3b and Table S1). There are some inverse relationships between PW and $-\omega$ (Figure 3c); much of the United States east of the Cascade and Sierra Nevada Mountains has negative correlations. As a result, only 3% of the stations have simultaneous statistically significant positive correlations between both EP and PW and EP and $-\omega$ (Table S1). The large areas of negative correlations of PW with $-\omega$ in southeastern regions where PW is largest suggest that thermodynamic, rather than dynamic, effects are driving the nonlinear behavior at the highest values of EP and PW. PW and $-\omega$ are not in synchrony when considering the most extreme EP events. This is further supported by the mixed set of positive and negative correlations when \mathbf{A} is correlated with $-\omega$ (Figure 3d).

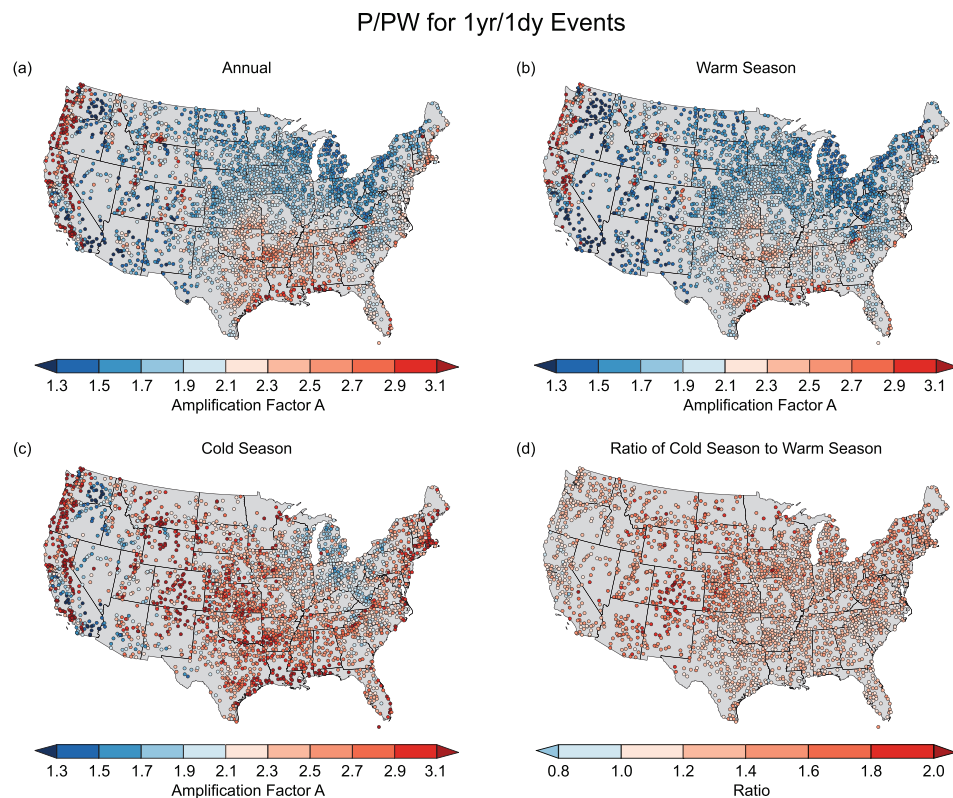


Figure 4. Average amplification factor (\mathbf{A}) for each station for precipitation events exceeding the 1-yr, 1-day threshold for (a) annual, (b) warm season, (c) cold season, and (d) cold to warm season ratio of \mathbf{A} .

3.4. Regionally Varying Weather Disturbances and their Role in EP Events

For a similar set of EP events used here, Kunkel et al. (2012) found that large-scale weather systems, including tropical and extratropical cyclones (and their associated fronts), were directly linked to most EP events. So there can be no doubt that dynamics related to values of ω are critically important but only after considerations of advection of moisture to achieve and sustain high values of PW. Through their circulation, dynamically forced weather systems can enhance local PW by proximity of locally available sources of moisture as well as their larger-scale moisture advection. This section explores this more fully.

Similar to the various correlations depicted in Figure 3 there is considerable spatial variability in \mathbf{A} (Figure 4a). This provides some useful clues to the interplay of dynamics, terrain, and q as it affects extreme precipitation amounts. High values of \mathbf{A} are found along the West Coast (particularly in the Sierra Nevada and Cascade Mountain Ranges), along the Gulf coast, and in the southern Appalachian Mountains. The high values in mountainous areas likely reflect enhanced convergence from topographic uplift. Lower values are found in the north central United States and intermontane areas of the West, quite similar to the pattern of negative correlations of PW with $-\omega$.

The values of \mathbf{A} are higher in the cold season compared to the warm season almost everywhere (Figures 4b–4d), pointing to the importance of organized dynamical weather systems and their related vertical motion and moisture transports when PW tends to be lower (Figure S3). This reflects the strength of the dynamical forcing in cold season compared to the significantly larger thermodynamic effects from ample local values of PW in the warm season. This is also indirect evidence that atmospheric overturning is important as the organized dynamical systems can enhance long-range and sustained transport of q over longer times. The high relative values of \mathbf{A} in the Sierra Nevada, Cascade, and extreme Southern Appalachian Mountains during both cold and warm seasons suggest that the dynamics of generally weaker warm season synoptic-scale systems can be strongly enhanced by abrupt orographic changes.

The relatively large warm season values of \mathbf{A} along and near the Gulf and Atlantic coastlines (Figure 4b), where tropical cyclones can be strong, suggest that those dynamical systems might also play an important role in enhancing \mathbf{A} to values up to 3. Cold season dynamics contribute significantly more than warm season dynamics as indicated by the large number of cold to warm season ratios of \mathbf{A} exceeding 1 (Figure 4d).

The climatology of weather types and their relationship to extreme precipitation events as developed by Kunkel et al. (2012) can be used to better understand and help interpret the values of \mathbf{A} regionally and seasonally. Kunkel et al. (2012) use the standard four seasons (December, January, February for winter, etc.) so the transition seasons were asymmetrically weighted when compared to the seasons used here. They assigned weather types to daily 5-yr return period extreme precipitation events, rarer than the 1-yr return interval used herein. The implication of this difference is expected to be modest at most (Kunkel et al., 2020). A regional decomposition of \mathbf{A} by region and season is provided in the supporting information (Text S2). The salient points include (1) EP events across each season and region are associated with different weather disturbances and these in turn can strongly affect regional and seasonal \mathbf{A} ; (2) large-scale synoptic weather types during the cold season coincide with both the high values of \mathbf{A} with relatively low PW as well as the apparent sub-CC relationship at low values of PW; and (3) in spite of large values of \mathbf{A} associated with strong dynamical effects, in the absence of strong orographic effects or close proximity to the coast, the amount of PW, and its associated thermodynamics, dictate the time of year with the highest EP.

4. Discussion and Conclusions

A central question for future design values of extreme precipitation relates to the role of q and its associated thermodynamic effects on extreme precipitation. Historically, both the probability of an extreme precipitation event and the spatial extent of extreme occurrences increase with PW (Figures 2, 3, and S5), but the interplay between thermodynamic and dynamic effects reflected in the amplification factor, \mathbf{A} , complicates a simple interpretation. On average, a value of \mathbf{A} of 2 is found for precipitation events exceeding the threshold for PDS and AMS events. It is common to find the \mathbf{A} as high as 3 or more, or as low as 1, depending on the local dynamics from orography or the types of atmospheric circulation affecting a region. For the highest (lowest) values of PW, \mathbf{A} increases (decreases) at a nonlinear rate.

The incorporation of global warming considerations into future design values for extreme precipitation, including IDF relationships and Probable Maximum Precipitation (PMP), is strongly motivated by the CC relationship and the large-scale model-simulated projected increases in PW (Kunkel et al., 2013). So any compensating dynamic effects from changes in weather dynamics will need to reverse the correlations between PW and $-\omega$; otherwise changes in EP amounts are likely to scale positively and nonlinearly at the highest values of PW. For the subset of the most extreme precipitation events analyzed here, there is often an opposing relationship between PW and $-\omega$ and EP and $-\omega$, suggesting that presently, PW is the limiting factor for EP amounts given modest thresholds of $-\omega$. Kunkel et al. (2013) found that future maximum PW increased with temperature at the CC rate or higher. Combined with our finding of increasing \mathbf{A} at high PW, this suggests that future changes in extreme precipitation are likely to be super CC.

There are a few ways in which future analyses could improve understanding. First, in order to ensure adequate spatial density, this analysis was limited to daily precipitation amounts and did not incorporate sub-daily data of particular interest for practical and theoretical reasons. Second, it would be useful to explore whether the behavior of \mathbf{A} calculated here is extensible across other time integration periods, for example, subdaily or multiday. There is some indication that they may be extensible because the correlations of PW versus EP (Figure 3) are similar for multiday versus 1-day extreme events across the United States. Lastly, the ideal characterization of the effect of q on extreme precipitation events would explicitly consider other factors such as orography, synoptic weather type, and the vertical structure of the q and vertical velocity. Consideration of these factors would likely provide additional insights regarding the synoptic climatology of current and future extreme precipitation events.

References

- Ban, N., Schmidli, J., & Schär, C. (2015). Heavy precipitation in a changing climate: Does short-term summer precipitation increase faster? *Geophysical Research Letters*, 42, 1165–1172. <https://doi.org/10.1002/2014GL062588>

- Bao, J., Sherwood, S. C., Alexander, L. V., & Evans, J. P. (2017). Future increases in extreme precipitation exceed observed scaling rates. *Nature Climate Change*, 7(2), 128–132. <https://doi.org/10.1038/NCLIMATE3201>
- Bao, J., Sherwood, S. C., Colin, M., & Dixit, V. (2017). The robust relationship between extreme precipitation and convective organization in idealized numerical modeling simulations. *Journal of Advances in Modeling Earth Systems*, 9(6), 2291–2303. <https://doi.org/10.1002/2017MS001125>
- Boessenkool, B., Bürger, G., & Heistermann, M. (2017). Effects of sample size on estimation of rainfall extremes at high temperatures. *Natural Hazards and Earth System Sciences*, 17(9), 1623–1629. <https://doi.org/10.5194/nhess-17-1623-2017>
- Bonnin, G.M., D. Martin, B. Lin, Parzybok T., Yekta M., and Riley D. (2004). Precipitation-frequency atlas of the United States volume 1 version 5.0: Semiarid southwest (Arizona, Southeast California, Nevada, New Mexico, Utah). NOAA Atlas 14, 271 pp.
- Chan, S. C., Kendon, E. J., Roberts, N. M., Fowler, H. J., & Blenkinsop, S. (2016). Downturn in scaling of UK extreme rainfall with temperature for future hottest days. *Nature Geoscience*, 9(1), 24–28. <https://doi.org/10.1038/ngeo2596>
- Dong, W., Lin, Y., Wright, J. S., Xie, Y., Yin, X., & Guo, J. (2019). Precipitable water and CAPE dependence of rainfall intensities in China. *Climate Dynamics*, 52(5–6), 3357–3368. <https://doi.org/10.1007/s00382-018-4327-8>
- Durre, I., Menne M. J., Gleason B. E., Houston T. G., & Vose R. S. (2010). Comprehensive Automated Quality Assurance of Daily Surface Observations. *Journal of Applied Meteorology and Climatology*, 49, (8), 1615–1633. <https://doi.org/10.1175/2010jamc2375.1>
- Durre, I., Menne, M. J., & Vose, R. S. (2008). Strategies for evaluating quality assurance procedures. *Journal of Applied Meteorology and Climatology*, 47(6), 1785–1791. <https://doi.org/10.1175/2007JAMC1706.1>
- Easterling, D. R., Kunkel, K. E., Arnold, J. R., Knutson, T., LeGrande, A. N., Leung, L. R., et al. (2017). Precipitation change in the United States. In D. J. Wuebbles, D. W. Fahey, K. A. Hibbard, D. J. Dokken, B. C. Stewart, & T. K. Maycock (Eds.), *Climate science special report: Fourth national climate assessment* (Vol. 1, pp. 207–230). Washington, DC, USA: United States Global Change Research Program. <https://doi.org/10.7930/J0H993CC>
- Emori, S., & Brown, S. J. (2005). Dynamic and thermodynamic changes in mean and extreme precipitation under changed climate. *Geophysical Research Letters*, 32, e315. <https://doi.org/10.1029/2005GL023272>
- Gelaro, R., McCarty, W., Suárez, M. J., Todling, R., Molod, A., Takacs, L., et al. (2017). The Modern-Era Retrospective Analysis for Research and Applications, Version 2 (MERRA-2). *Journal of Climate*, 30(14), 5419–5454. <https://doi.org/10.1175/JCLI-D-16-0758.1>
- Giorgi, F., Raffaele, F., & Coppola, E. (2019). The response of precipitation characteristics to global warming from climate projections. *Earth System Dynamics*, 10(1), 73–89. <https://doi.org/10.5194/esd-10-73-2019>
- Groisman, P. Y., Knight, R. W., Easterling, D. R., Karl, T. R., Hegerl, G. C., & Razuvaev, V. N. (2005). Trends in intense precipitation in the climate record. *Journal of Climate*, 18(9), 1326–1350. <https://doi.org/10.1175/JCLI3339.1>
- Hoerling, M., Eischeid, J., Perlitz, J., Quan, X., Wolter, K., & Cheng, L. (2016). Characterizing recent trends in U.S. heavy precipitation. *Journal of Climate*, 29(7), 2313–2323. <https://doi.org/10.1175/JCLI-D-15-0441.1>
- Huang, D., Yan, P., Xiao, X., Zhu, J., Tang, X., Huang, A., & Cheng, J. (2019). The tri-pole relation among daily mean temperature, atmospheric moisture and precipitation intensity over China. *Global and Planetary Change*, 179, 1–9. <https://doi.org/10.1016/j.gloplacha.2019.04.016>
- IPCC (2013). In T. F. Stocker, D. Qin, G.-K. Plattner, M. Tignor, S. K. Allen, J. Boschung, A. Nauels, Y. Xia, V. Bex, & P. M. Midgley (Eds.), *Climate change 2013: The physical science basis. Contribution of Working Group I to the Fifth Assessment Report of the Intergovernmental Panel on Climate Change*, (p. 1535). Cambridge, United Kingdom and New York, NY, USA: Cambridge University press. <https://doi.org/10.1017/CBO9781107415324>
- Kalnay, E., Kanamitsu, M., Kistler, R., Collins, W., Deaven, D., Gandin, L., et al. (1996). The NCEP/NCAR 40-year reanalysis project. *Bulletin of the American Meteorological Society*, 77(3), 437–471. [https://doi.org/10.1175/1520-0477\(1996\)077<0437:TNYRP>2.0.CO;2](https://doi.org/10.1175/1520-0477(1996)077<0437:TNYRP>2.0.CO;2)
- Karl, T. R., & Knight, R. W. (1998). Secular trends of amount frequency, and intensity of precipitation across the United States. *Bulletin of the American Meteorological Society*, 79(2), 231–241. [https://doi.org/10.1175/1520-0477\(1998\)079<0231:STOPAF>2.0.CO;2](https://doi.org/10.1175/1520-0477(1998)079<0231:STOPAF>2.0.CO;2)
- Karl, T. R., & Koscielny, A. J. (1982). Drought in the United States: 1894–1981. *International Journal of Climatology*, 2(4), 313–329. <https://doi.org/10.1002/joc.3370020402>
- Karl, T. R., Williams, C. N. Jr., Young, P. J., & Wendland, W. M. (1986). A model to estimate the time of observation bias associated with monthly mean maximum, minimum, and mean temperature for the United States. *Journal of Climate and Applied Meteorology*, 25(2), 145–160. [https://doi.org/10.1175/1520-0450\(1986\)025<0145:AMTETT>2.0.CO;2](https://doi.org/10.1175/1520-0450(1986)025<0145:AMTETT>2.0.CO;2)
- Kitoh, A., & Endo, H. (2016). Changes in precipitation extremes projected by a 20-km mesh global atmospheric model. *Weather and Climate Extremes*, 11, 41–52. <https://doi.org/10.1016/j.wace.2015.09.001>
- Kunkel, K. E., Easterling, D. R., Kristovich, D. A. R., Gleason, B., Stoecker, L., & Smith, R. (2012). Meteorological causes of the secular variations in observed extreme precipitation events for the conterminous United States. *Journal of Hydrometeorology*, 13(3), 1131–1141. <https://doi.org/10.1175/JHM-D-11-0108.1>
- Kunkel, K. E., Karl, T. R., Easterling, D. R., Redmond, K., Young, J., Yin, X., & Hennon, P. (2013). Probable maximum precipitation (PMP) and climate change. *Geophysical Research Letters*, 40, 1402–1408. <https://doi.org/10.1002/grl.50334>
- Kunkel, K. E., Karl, T. R., Squires, M. F., Yin, X., Stegall, S. T., & Easterling, D. R. (2020). Precipitation extremes: Trends and relationships with average precipitation and precipitable water in the contiguous United States. *Journal of Applied Meteorology and Climatology*, 59(1), 125–142. <https://doi.org/10.1175/JAMC-D-19-0185.1>
- Lavers, D. A., Pappenberger, F., Richardson, D. S., & Zsoter, E. (2016). ECMWF extreme forecast index for q transport: A forecast tool for atmospheric rivers and extreme precipitation. *Geophysical Research Letters*, 43, 11,852–11,858. <https://doi.org/10.1002/2016GL071320>
- Mahoney, K., Lukas J., and Mueller M. (2018). Summary report Volume VI Considering climate change in the estimation of extreme precipitation for dam safety. Colorado Division of Water Resources, Dept of Natural Resources (pp. 57).
- Menne, M. J., Durre, I., Vose, R. S., Gleason, B. E., & Houston, T. G. (2012). An overview of the global historical climatology network-daily database. *Journal of Atmospheric and Oceanic Technology*, 29, 897–910. <https://doi.org/10.1175/JTECH-D-11-00103.1>
- Nie, J., Sobel, A. H., Shaevitz, D. A., & Wang, S. (2018). Dynamic amplification of extreme precipitation sensitivity. *PNAS*, 115(38), 9467–9472. <https://doi.org/10.1073/pnas.1800357115>
- O'Gorman, P., & Schneider, T. (2009). The physical basis for increases in precipitation extremes in simulation of 21st-century climate change. *PNAS*, 106, 14,773–14,777.
- Perica, S., Pavlovic, S., St. Laurent, M., Trypaluk C., Unruh D., & Wihite O. (2018). NOAA Atlas 14 precipitation-frequency atlas of the United States Volume 11 Version 2.0: Texas, Library of Congress classification number G1046.C8 U6 no.14 v.11 (2018). https://www.nws.noaa.gov/oh/hdsc/PF_documents/Atlas14_Volume11.pdf
- Prein, A. F., & Pendergrass, A. G. (2019). Can We Constrain Uncertainty in Hydrologic Cycle Projections? *Geophysical Research Letters*, 46, 3911–3916.

- Schroeder, K., & Kirchengast, G. (2018). Sensitivity of extreme precipitation to temperature: The variability of scaling factors from a regional to local perspective. *Climate Dynamics*, 50(11-12), 3981–3994. <https://doi.org/10.1007/s00382-017-3857-9>
- Sillmann, J., Karin, V. V., Zwiers, F. W., Zhang, X., & Bronaugh, D. (2013). Climate extremes indices in the CMIP5 multimodel ensemble: Part 2. Future climate projections. *Journal of Geophysical Research: Atmospheres*, 118, 2473–2493. <https://doi.org/10.1002/jgrd.50188>
- Sugiyama, M., Shiogama, H., & Emori, S. (2010). Precipitation extreme changes exceeding moisture content increases in MIROC and IPCC climate models. *PNAS*, 107(2), 571–575. <https://doi.org/10.1073/pnas.0903186107>
- Thackeray, C. W., DeAngelis, A. M., Hall, A., Swain, D. L., & Qu, X. (2018). On the connection between hydrologic sensitivity and regional wet extremes. *Geophysical Research Letters*, 45, 11,343–11,351. <https://doi.org/10.1029/2018GL079698>
- Trenberth, K. E., Dai, A., Rasmusson, R. M., & Parsons, D. B. (2003). The changing character of precipitation. *Bulletin of the American Meteorological Society*, 84(9), 1205–1218.
- Wang, G., Wang, D., Trenberth, K. E., Erfanian, A., Yu, M., Bosilovich, M. G., & Parr, D. T. (2017). The peak structure and future changes of the relationships between extreme precipitation and temperature. *Nature Climate Change*, 7(4), 268–274. <https://doi.org/10.1038/nclimate3239>
- Wright, D. B., Bosma, C. D., & Lopez-Cantu, T. (2019). U.S. hydrologic design standards insufficient due to large increases in frequency of rainfall extremes. *Geophysical Research Letters*, 46, 8144–8153. <https://doi.org/10.1029/2019GL08323>
- Ye, H., Fetzer, E. J., Wong, S., Behrangi, A., Yang, D., & Lambrightson, B. H. (2015). Increasing atmospheric q and higher daily precipitation intensity over northern Eurasia. *Geophysical Research Letters*, 42, 9404–9410. <https://doi.org/10.1002/2015GL066104>
- Ye, H., Fetzer, E. J., Wong, S., & Lambrightson, B. H. (2017a). Rapid decadal convective precipitation increases over Eurasia during the last three decades of the 20th century. *Science Advances*, 3(1), e1600944. <https://doi.org/10.1126/sciadv.1600944>
- Ye, H., Fetzer, E. J., Wong, S., Lambrightson, B. H., Wang, T., Chen, L., & Dang, V. (2017b). More frequent showers and thunderstorm days under a warming climate: Evidence observed over northern Eurasia from 1966 to 2000. *Climate Dynamics*, 49(5-6), 1933–1944. <https://doi.org/10.1007/s00382-016-3412-0>